Published in final edited form as:
Cell Mol Neurobiol. 2008 December ; 28(8): 1079–1093. doi:10.1007/s10571-008-9285-y.

Combining Voltage and Calcium Imaging from Neuronal Dendrites

Marco Canepari,
Department of Pharmacology and Neurobiology, University of Basel, Klingelbergstrasse 70, 4056 Basel, Switzerland

Department of Cellular and Molecular Physiology, Yale University School of Medicine, New Haven, CT 06520, USA

Kaspar Vogt, and
Department of Pharmacology and Neurobiology, University of Basel, Klingelbergstrasse 70, 4056 Basel, Switzerland

Dejan Zecevic
Department of Cellular and Molecular Physiology, Yale University School of Medicine, New Haven, CT 06520, USA

Abstract

The ability to monitor membrane potential (V_m) and calcium (Ca^{2+}) transients at multiple locations on the same neuron can facilitate further progress in our understanding of neuronal function. Here we describe a method to combine V_m and Ca^{2+} imaging using styryl voltage sensitive dyes and Fura type UV-excitable Ca^{2+} indicators. In all cases V_m optical signals are linear with membrane potential changes, but the calibration of optical signals on an absolute scale is presently possible only in some neurons. The interpretation of Ca^{2+} optical signals depends on the indicator Ca^{2+} buffering capacity relative to the cell endogenous buffering capacity. In hippocampal CA1 pyramidal neurons, loaded with JPW-3028 and 300 μM Bis-Fura-2, V_m optical signals cannot be calibrated and the physiological Ca^{2+} dynamics are compromised by the presence of the indicator. Nevertheless, at each individual site, relative changes in V_m and Ca^{2+} fluorescence signals under different conditions can provide meaningful new information on local dendritic integration. In cerebellar Purkinje neurons, loaded with JPW-1114 and 1 mM Fura-FF, V_m optical signals can be calibrated in terms of mV and Ca^{2+} optical signals quantitatively reveal the physiological changes in free Ca^{2+}. Using these two examples, the method is explained in detail.

Keywords

Voltage-sensitive dyes; Calcium-sensitive dyes; Imaging; Neuronal dendrites

Introduction

Membrane potential (V_m) and intracellular calcium (Ca^{2+}) transients are the basic signalling mechanisms in nerve cells. Thus, an optical technique that allows monitoring both signals at

Correspondence to: Marco Canepari.
marco.canepari@unibas.ch .

multiple locations on the same neuron can significantly improve our capability to investigate and understand neuronal function.

The initial idea of multiple-site optical recording of membrane potential transients (voltage imaging) from individual nerve cells using selective staining of neurons by intracellular application of voltage sensitive dyes (Cohen et al. 1974; Grinvald et al. 1987) was further developed, first in invertebrate neurons in isolated ganglia (Antic and Zecevic 1995; Zecevic 1996; Antic et al. 2000) and subsequently adopted for mammalian nerve cells in brain slices (Antic et al. 1999; Antic 2003; Djurisic et al. 2004). Numerous analogues of the most successful voltage sensitive dyes were tested for intracellular application (Grinvald et al. 1987; Antic and Zecevic 1995). Presently, the optimal voltage indicators in recording from neuronal processes of individual neurons in brain slices are a fluorescent dye designated JPW-1114 (also called di-2-ANEPEQ; available from Invitrogen—Molecular Probes) and its close analogue JPW-3028 (di-1-ANEPEQ) (Djurisic et al. 2004; Milojkovic et al. 2005; Palmer and Stuart 2006; Berger et al. 2007; Gasparini et al. 2007; Canepari et al. 2007). These dyes are lipophilic but still sufficiently water soluble to be used for micro-injection. Both dyes belong to aminostyryl pyridinium class of fast potentiometric membrane dyes that undergo a large charge shift upon excitation and display a strictly linear electrochromic response to membrane potential in the range of −100 mV to 100 mV (Loew and Simpson 1981; Loew et al. 1992). The excitation wavelengths used for V_m imaging for this dye are in the range of 520 ± 45 nm. Similar sensitivity was recently reported for a new series of styryl electrochromic dyes developed to extend the excitation wavelength from 450 to 550 nm range to wavelengths close to 700 nm (Zhou et al. 2007).

If a neuron is stained with two indicators with different spectral properties, the time course of two independent physiological variables can be monitored at the same locations in the same experiment and directly correlated. The possibility to combine optical recordings using two indicators has been utilised to measure intracellular pH and Ca^{2+} (Martinez-Zaguilan et al. 1991) and slow membrane potential changes and Ca^{2+} signals (Kremer et al. 1992). For combined fast V_m and Ca^{2+} optical recordings, because the best-known styryl dyes are characterised by broad excitation and emission spectra, the choice of a specific Ca^{2+} indicator is limited. One possibility is to use blue-excitable green-fluorescent Ca^{2+} indicators (i.e. Fluo, Calcium Green and Oregon Green indicators) as reported by Bullen and Saggau (1998) and by Berger et al. (2007) or green-excitable orange-fluorescent Ca^{2+} indicators (Sinha and Saggau 1999). The use of these Ca^{2+} indicators in combination with styryl dyes has two main disadvantages. First, because of the large overlap in the excitation spectra and the still significant overlap in the emission spectra of the voltage and Ca^{2+} indicators, Ca^{2+} related fluorescence signals can be contaminated by the fluorescence from the voltage sensitive dye (unpublished observations). Second, since the wavelengths that are used to excite the Ca^{2+} indicator are strongly absorbed by the voltage sensitive dye, Ca^{2+} measurements contribute to the photo-damage caused by the voltage sensitive dye. To minimise these problems, combined V_m and Ca^{2+} imaging can be done using UV-excitable Ca^{2+} indicators such as Bis-Fura-2, as described in our recent study (Canepari et al. 2007) and by Milojkovic et al. (2007). In principle, Ca^{2+} signals with similar optical properties can be obtained using anyone of the commercially available UV-excitable Fura dyes (Fura-2, Bis-Fura-2, Fura-4F, Fura-5F, Fura-6F, Fura-FF and Mag-Fura-2).

Although the use of UV-excitable Ca^{2+} indicators provides independent V_m and Ca^{2+} fluorescent signals, combining V_m and Ca^{2+} imaging have limitations that depend on neuronal properties. In voltage imaging, an important factor is the ability to calibrate signals in terms of membrane potential (in mV). In some neurons this calibration is possible because a voltage signal of known amplitude is available at every recording site and can be used as a calibration standard. For example, in mitral cells of the olfactory bulb the axo-somatic action

potentials are known to propagate without attenuation along the dendritic arbor (Bischofberger and Jonas 1997) and were used to calibrate V_m optical recordings (Djurisic et al. 2004). In cerebellar Purkinje neurons such a calibration could be accomplished using a prolonged hyperpolarisation generated in the soma which spreads with little attenuation along the dendritic tree (Stuart and Häusser 1994). In the majority of the neurons, however, a calibrating signal is not available and the amplitude of V_m optical signals from different sites cannot be quantitatively compared. Nevertheless, at each individual site, V_m optical signals still vary as a linear function of the membrane potential change. This signal can be used for providing spatially well-resolved analysis of relative changes in membrane potential responses under different conditions. Additionally, an approximate calibration of optical signals on an absolute scale is possible in many parts of the dendritic arbor of several principal neuronal types. Such a calibration is based on the known absolute amplitude of the decremental back-propagating action potential in different parts of the dendritic tree (e.g. Frick et al. 2004).

The interpretation of Ca^{2+} optical signals depends on the Ca^{2+} buffering capacity of the indicator relative to the endogenous buffering capacity of the cell. At one extreme, if the Ca^{2+} buffering capacity of the dye is significantly higher than the endogenous Ca^{2+} buffering capacity of the cell, the physiological Ca^{2+} homeostasis is altered by the presence of the indicator and the quantitative estimation of intracellular free Ca^{2+} concentration becomes meaningless (Nowycky and Pinter 1993). Nevertheless, Ca^{2+} optical signals will still reflect the kinetics of the dye-bound Ca^{2+} and can serve as an estimate of the total intracellular Ca^{2+} increase. At the opposite extreme, if the buffering capacity of an indicator is so low that its presence does not significantly alter the physiological Ca^{2+} homeostasis, Ca^{2+} optical signals can be used to measure intracellular free Ca^{2+} changes at any location with minimal distortion by diffusion of the dye-bound Ca^{2+}.

In this report, we illustrate the method of combined V_m and Ca^{2+} imaging by two indicative examples. In the first example, we explore hippocampal CA1 pyramidal neurons in which V_m signals cannot be precisely calibrated and the dye Ca^{2+} buffering capacity dominates the relatively low endogenous Ca^{2+} buffering of the neuron. In the second example we explore cerebellar Purkinje neurons in which V_m optical signals can be calibrated and the dye Ca^{2+} buffering is negligible compared to the relatively high endogenous Ca^{2+} buffering of the cell.

Methods

Slice Preparation

Experiments on hippocampal CA1 pyramidal neurons were carried out on hippocampal slices from 21- to 30-day-old Sprague–Dawley rats. The rats were decapitated following halothane anaesthesia and 300 μm thick slices were cut as described in Canepari et al. (2007). Slices were incubated at 37°C for 30 min and then maintained at room temperature (23–25°C). Measurements were done at 33–35°C. The extracellular solution used during slicing, incubation and recording contained (in mM): 125 NaCl, 26 $NaHCO_3$, 20 glucose, 2.5 KCl, 1.25 NaH_2PO_4, 2 $CaCl_2$ and 1 $MgCl_2$, and was bubbled with gas mixture (95% O_2, 5% CO_2).

Experiments on cerebellar Purkinje Neurons were done in 250 μm thick sagittal cerebellar slices from 25 to 35 days old mice (C57BL/6). Animals were decapitated following enflurane anaesthesia (all experiments were performed in accordance with the Swiss regulations for animal experimentation) and slices were prepared in ice-cold solution using a HM 650 V vibroslicer (Microm, Germany). Slices were incubated at 35°C for 40 min and thereafter maintained at room temperature (23–25°C). Measurements were done at 32–34°C.

The extracellular solution used during incubation and recording contained (in mM): 125 NaCl, 26 $NaHCO_3$, 20 glucose, 3 KCl, 1 NaH_2PO_4, 2 $CaCl_2$ and 1 $MgCl_2$, pH 7.4 when bubbled with gas mixture (95% O_2, 5% CO_2). The solution used for slicing contained 0.4 mM $CaCl_2$ and in some animals 250 mM sucrose replaced NaCl.

Electrophysiological Recordings

Somatic whole-cell recordings were made with a Multiclamp 700A amplifier (Axon Instruments, USA) under visual control using infrared DIC video-microscopy on an upright microscope (Model BX51-WI, Olympus, Japan). The basic intracellular solution contained (mM): 120 $KMeSO_4$, 10 NaCl, 4 Mg-ATP, 0.3 Tris-GTP, 14 Tris-Phosphocreatine, 20 HEPES (pH 7.3, adjusted with KOH). Dyes (all purchased from Molecular Probes—Invitrogen, Carlsbad, CA, USA, except JPW-3028 obtained from Leslie Loew and Joe Wuskell of the University of Connecticut) were dissolved in water and added to their final concentration of 0.25–1 mg/ml for the voltage sensitive dyes. The procedure of staining individual neurons with voltage sensitive dyes is described in the first part of the result section. Local stimulation of presynaptic fibres was carried out with patch pipettes filled with extracellular solution positioned using hydraulic manipulators (Narishige, Japan).

Imaging Apparatus and Data Analysis

The schematic of the imaging apparatus is shown in Fig. 1. The source of excitation light was either a 250 W xenon arc lamp powered by Model 1700XT/A power supply (Opti-Quip, Highland Mills, NY, USA) or a 150 W xenon lamp (CAIRN Research Ltd., Faversham, UK). The light was directed either to a filter cube for the voltage sensitive dye or to another cube optimised for the Ca^{2+} indicator. The cubes were inserted in the light pathway with a manual switch. The JPW filter cube had an excitation band-pass filter ex1 = 525 ± 25 nm, a dichroic mirror dic1 > 570 nm and a long-pass emission filter em1 > 610 nm. The Fura filter cube had a band-pass excitation filter ex2 = 387 ± 6 nm, a dichroic mirror dic1 > 470 nm and a band-pass emission filter em1 = 510 ± 42 nm. The excitation light from the filter cube was further directed to a water immersion objective (either Nikon 60X/1.0 NA or Olympus 60X/1.1 NA) to illuminate the preparation, and the fluorescent image of the stained cell was projected via an optical coupler (either 0.1X for hippocampal CA1 pyramidal neurons or 0.25X for cerebellar Purkinje neurons) onto a CCD chip of a Neuro-CCD-SM (RedShirtImaging LLC, Decatur, GA, USA). The imaged field was ~300 μm × 300 μm and ~125 μm× 125 μm in measurements from hippocampal CA1 pyramidal neurons or from cerebellar Purkinje neurons, respectively. The NeuroCCD-SM CCD is a fast data acquisition camera with 80 × 80 pixels designed primarily for voltage imaging. The camera can acquire up to 2,000 frames/s at full-frame resolution. In Ca^{2+} measurements, images were acquired at 500 frames/s. V_m signals were acquired either at 2,000 frames/s or at 5,000 frames/s (binning factor 3). During the experiment, individual trials were saved and checked for consistency. This was necessary to correlate V_m and Ca^{2+} signals and average trials in order to increase the signal-to-noise ratio. Data were analysed either with NeuroPlex (RedShirtImaging LLC, Decatur, GA, USA) or with dedicated software written in Matlab (The MathWorks Inc., Natick, MA, USA).

Pharmacological Effects and Photodynamic Damage of JPW-1114 at Cerebellar Purkinje Neurons

Cell overload with voltage sensitive dyes or excessive exposures to light can cause pharmacological effects and photodynamic damage. Previous studies have shown that voltage sensitive dyes JPW-1114 or JPW-3028 have little pharmacological effect when applied at functional concentrations to vertebrate neurons. Staining and a moderate number of repetitive exposures to light had negligible effect on the size and waveform of action potentials elicited by somatic current injection in neocortical and CA1 hippocampal

pyramidal neurons and in mitral cells of the olfactory bulb (Antic et al. 1999; Antic 2003; Djurisic et al. 2004; Palmer and Stuart 2006; Canepari et al. 2007). We repeated the same test in cerebellar Purkinje neurons from the mouse. In four cells, stained at 32–34°C with JPW-1114, action potentials were recorded somatically at a sampling rate of 16 kHz during the staining, immediately after re-patching following equilibration of the dye inside the cell and after 20–25 light exposures lasting 150 ms and separated by 30 s time intervals. The summary results of this test are shown in Fig. 2a. The amplitude of the action potential relative to the initial amplitude (mean ± SD) was 0.98 ± 0.02 after re-patching and 0.97 ± 0.06 following the light exposures. The firing threshold relative to the initial one was 1.02 ± 0.05 after re-patching and 0.99 ± 0.08 following the light exposures. The width at half-height, typically 4–5 data points, changed at most one sample in either direction. Its value relative to the initial one was 1.06 ± 0.13 after re-patching and 1.02 ± 0.18 following the light exposures. The changes in these parameters were not significant ($P > 0.1$, paired *t*-test) demonstrating that pharmacological effects and photodynamic damage did not influence somatic action potentials in Purkinje neurons. In Purkinje neurons, somatic action potentials do not back-propagate to the dendrites (Stuart and Häusser 1994). In order to test the effects of the dye on dendritic signals, we measured the somatic climbing fibre excitatory postsynaptic potential (EPSP) and the associated Ca^{2+} signal in the dendrites during the staining, immediately after re-patching following equilibration of the dye and after 20 light exposures.

Ca^{2+} signals were estimated by averaging fluorescence over the entire imaged dendrite to minimise fluctuations due to local variability. The climbing fibre EPSP is an all-or-none synaptic potential enabling us to explore the pharmacological effects of JPW-1114 directly on synaptic signals at the site of origin. In order to prevent somatic firing associated with the climbing fibre EPSP, this test was done with 10 mM of the Na^+ channel blocker QX-314 in the internal solution. The summary of the results is shown in Fig. 2b. The amplitudes of the EPSP and Ca^{2+} signal, relative to their initial values, were 1.00 ± 0.02 and 0.99 ± 0.10 after re-patching and 0.97 ± 0.06 and 1.06 ± 0.08 after 20 light exposures ($N = 5$ cells, $P > 0.1$ in all paired *t*-tests). We concluded that the voltage sensitive dye did not significantly affect excitatory synaptic transmission and dendritic excitability in cerebellar Purkinje neurons.

Results

Staining of the Cells and Recording Procedures—The staining protocol for a cerebellar Purkinje neuron is illustrated in Fig. 3a. Intracellular staining was accomplished by free diffusion of the dyes from a patch-electrode into the soma in 15–60 min, depending on the electrode resistance. Glass pipettes were first filled from the tip with dye-free solution by applying negative pressure for about 1 min and then back-filled with the solution containing the two indicators. Dye-free solution in the tip was necessary to prevent the leakage of the dye into the extracellular medium before the electrode is attached to the neuron.

Although the equilibration of the Ca^{2+} indicator in distal dendrites takes longer than 20 min, Fura fluorescence over the entire dendritic field could be detected already after 5–10 min when JPW fluorescence was almost absent. JPW fluorescence in the soma was detectable after 10–20 min with the highest increase typically after 20–30 min. The patch electrode was detached from the cell by forming an outside-out patch after 30–45 min when the resting light intensity from the soma was measured using 0.75% of the total light intensity, in order to prevent pharmacological effects due to dye overload (Djurisic et al. 2004; Canepari et al. 2007). Presently, the signal-to-noise ratio for voltage imaging increases with the light intensity but is usually limited by the photodynamic damage. While there is a non-linear (third order) relation between the damage and the illumination intensity, there is a linear

relation between the damage and dye concentration (Sacconi et al. 2006). Thus, it is favourable to maximise staining. In hippocampal CA1 pyramidal neurons experiments, the dye diffusion from a patch-pipette into the cell body continued until the first change in the action potential shape was detected (30–45 min). The resting light intensity in the soma was then determined under standard recording conditions (2 KHz frame rate; 0.075% of the full excitation light intensity). In subsequent experiments we gradually extended the staining period to increase the amount of dye in the soma, as indicated by the resting light intensity, until irreversible damage to the neuron was caused. The damage was, most likely, caused by the non-specific pharmacological effects of the dye. In subsequent experiments, the staining was then adjusted to be slightly below the damaging concentration of the dye.

After that, the preparation was incubated for additional 1–2 h at room temperature to allow the voltage-sensitive dye to diffuse into distal processes. The position of the cell was localised within the slice using the voltage fluorescence and the cell body was usually re-patched before making optical measurements to obtain electrical recordings from the soma. Both the duration of staining and the equilibration period depend on temperature. Although these were faster at near physiological temperatures (32–34°), the survival of cells was better if the staining and the incubation were done at 24°. Thus, staining and incubation was routinely done at room temperature except in the experiments used to test the toxicity of the dye.

An example of V_m and Ca^{2+} optical signals obtained sequentially from the two indicators from three regions on the dendritic tree of a Purkinje neuron stained by JPW-1114 and Fura-FF is illustrated in Fig 3b. An intracellular calcium increase corresponds to a fractional decrease of fluorescence for a Fura dye excited at 387 nm (see methods). The signals were elicited by the activation of a climbing fibre EPSP. The signal-to-noise ratio in these recordings was improved by averaging four responses. Signal averaging as well as the sequential recording of V_m and Ca^{2+} signals is meaningful only if repeated application of the same stimulation protocol resulted in the same response. This was confirmed in measurements of the type shown in Fig. 3c. The V_m and the Ca^{2+} signals were recorded from a 10 × 10 μm location on the dendritic tree of a Purkinje cell in response to four repetitions of climbing fibre activation separated by 1 min. The results showed that signals were practically identical in four individual trials (grey traces). The superimposed black traces correspond to the averages of V_m and Ca^{2+} responses. Therefore, it was possible to directly compare V_m and Ca^{2+} signals recorded sequentially.

Interpretation of V_m and Ca^{2+} Optical Signals

In the general case, V_m optical signals cannot be calibrated on an absolute scale in terms of membrane potential. In a multi-site recording, the fractional change in light intensity is proportional to voltage, but also, to a different extent at different sites, to the ratio between the amount of dye that is bound to membranes that do not change potential (inactive dye) and the amount of dye that is bound to membranes that change potential (active dye). This ratio is unknown and varies in different regions of the neuron. Thus, the fractional change of fluorescence corresponding to a given membrane potential change is different in recording from different regions of the cell and the calibration of all detector pixels cannot be done by calibrating the optical signal from any single site.

Since the fractional change of fluorescence corresponding to a given membrane potential transient from a given site is fairly stable over many acquisition trials, such a calibration is absolute and straightforward if a calibrating electrical signal of known amplitude is available at all locations. An all-or-none action potential signal is ideal for this purpose and can be used to create a “sensitivity profile” of the neuron under study. This type of calibration was used to scale the amplitudes of optical signals from mitral cells (Djurisic et al. 2004). A

similar calibration is possible in the dendritic tree of Purkinje neurons using a long lasting hyperpolarising pulse which spreads into the dendritic arbor from the soma with little amplitude attenuation (Stuart and Häusser 1994). The same approach of calibrating V_m signals is not possible in hippocampal CA1 pyramidal neurons (Canepari et al. 2007) or in neocortical pyramidal neurons (Antic et al. 1999; Antic 2003) because a membrane potential transient of known amplitude is not available. Nevertheless, at each individual site, voltage imaging provides useful information on relative changes in membrane potential responses under different conditions.

The interpretation of Ca^{2+} optical signals depends on how much a Ca^{2+} indicator perturbs the physiological Ca^{2+} homeostasis. The buffering capacity of a Ca^{2+} indicator, K_{dye}, is defined as the ratio between the dye-bound Ca^{2+} and the free Ca^{2+} in the presence of the indicator. Some theoretical values of K_{dye} for the commercially available Fura dyes at the concentrations of 300 μM and 1 mM are shown in Table 1. The perturbation of the physiological Ca^{2+} introduced by the Ca^{2+} indicator can be evaluated by comparing the parameter K_{dye} with the endogenous buffering capacity of the cell (K_{cell}) which can be measured using standard procedures (Neher 1995). Table 2 shows some examples of estimates of K_{cell} that can vary among different systems by two orders of magnitudes. The parameter R_K, defined as the ratio between K_{dye} and K_{cell}, provides an estimate of the fraction of Ca^{2+} that binds to the indicator compared to the Ca^{2+} that binds to the endogenous buffer. The interpretation of Ca^{2+} optical signals is simplified in two extreme cases: $R_K >>$ and $R_K << 1$.

If $R_K >> 1$, it is possible to assume that Ca^{2+} will bind almost exclusively to the dye and the measurement of the physiological intracellular free Ca^{2+} is not possible in these conditions. If the Ca^{2+} indicator is not saturated, the total intracellular Ca^{2+} signal is given by the dye-bound Ca^{2+}

$$\Delta\left[DCa^{2+}\right] = [D] \cdot (F_{min} - F) / (F_{min} - F_{max}) \quad (1)$$

where $[D]$ is the total concentration of the dye, F is fluorescence and F_{min} and F_{max} are the fluorescence at 0 and saturating Ca^{2+} (Ogden and Capiod 1997; Canepari et al. 2004). The resting intracellular free Ca^{2+} concentration is very low and F_{min} can be approximated with the initial fluorescence (F_0). Since the auto-fluorescence of the slice can be typically used as a good estimate for F_{max}, $\Delta[DCa^{2+}]$ is proportional to the inverse fractional change in fluorescence after auto-fluorescence subtraction ($-\Delta F/F$). The spatio-temporal gradient of $-\Delta F/F$ reflects the binding of the Ca^{2+} to the dye and the diffusion of the dye-bound Ca^{2+} (Nowycky and Pinter 1993; Canepari and Mammano 1999). It follows that a signal that corresponds to a local increase in free Ca^{2+} concentration restricted to a particular site (for instance a dendritic spine) under physiological conditions, would be, in the presence of the indicator, observed elsewhere as result of the diffusion of $\Delta[DCa^{2+}]$ following a local increase in Ca^{2+}.

In the other extreme case of $R_K << 1$, the fraction of a Ca^{2+} transient that binds to the dye is negligible compared to the fraction bound to the endogenous buffering of the cell. Under these conditions, the estimate of the amplitude of the change in intracellular free Ca^{2+}, given by

$$\Delta\left[Ca^{2+}\right]_i = K_d \cdot (F_{min} - F) / (F - F_{max}) \quad (2)$$

will be veryclose tothe physiological one andwill also track the dynamics of intracellular free Ca^{2+} concentration. As in Eq. 1, $\Delta[Ca^{2+}]_i$ can be approximated with $K_d \cdot (F_0 - F)/(F)$ where F_0 is the initial (steady-state) fluorescence.Under these conditions, Ca^{2+} signals can be directly related to the physiological functions of a neuron.

The following two examples describe the application of V_m and Ca^{2+} imaging in preparations where optical signals can either be used to indicate relative changes under different experimental conditions or can be calibrated on the absolute scale.

Combined Voltage and Ca^{2+} Imaging from Hippocampal CA1 Pyramidal Neurons

In measurements from CA1 pyramidal neurons, we loaded individual neurons with the voltage-sensitive dye JPW-3028 and 300 μM Bis-Fura-2 to analyse, over large regions of the dendritic tree, the V_m and Ca^{2+} signals responsible for the induction of LTP. As stated above, V_m optical signals from the dendritic tree of hippocampal CA1 pyramidal neurons cannot be precisely calibrated in terms of mV. These cells are also characterised by relatively low endogenous buffering capacity in the dendrites and even lower buffering capacity in the spines (Table 2). Thus, in order to preserve physiological Ca^{2+} homeostasis, sub-millimolar concentrations of low affinity Fura dyes (Fura-6F, Fura-FF or Mag-Fura-2) would have to be used. However, these dyes cannot reliably measure Ca^{2+} transients that, under physiological conditions, correspond to a $\Delta[Ca^{2+}]_i$ substantially lower than 1 μM, such as those associated with back-propagating action potentials. Therefore, reliable measurements of small Ca^{2+} transients from hippocampal CA1 pyramidal neurons required application of Bis-Fura-2, a higher affinity indicator dye.

Figure 4 shows typical measurements from a hippocampal CA1 pyramidal neuron. The sensitivity of V_m and Ca^{2+} imaging from an apical dendrite is illustrated in panels (b) and (c). Optical signals correspond to a back-propagating action potential evoked in the soma by a depolarising current pulse. V_m signals declined in amplitude with distance from the soma and became undetectable in dendritic regions that were more than 400 μm away from the cell body (Fig. 4b). The amplitude of V_m signals from different locations, however, can be compared only approximately because the optical signals could not be precisely calibrated. Ca^{2+} transients associated with the back-propagating action potential, recorded from the same dendritic regions, also declined in amplitude with distance from the soma (Fig. 4c). The relatively small fractional change in fluorescence (<2%) indicates that Ca^{2+} influx associated with a back-propagating action potential did not saturate the indicator and that the signal was proportional to the integral of the Ca^{2+} flux (e.g. Helmchen et al. 1996). However, since the Ca^{2+} entering the cell was almost exclusively sequestrated by the indicator, these measurements could not be used to estimate the physiological Ca^{2+} dynamics. With these limitations in quantifying optical signals, our measurements are still qualitatively consistent with previous studies showing that the amplitude of the back-propagating action potential, as well as the associated Ca^{2+} transient, declined monotonically with distance from the soma along the distal part (>200 μm from soma) of the main apical dendrite (Jaffe et al. 1992; Spruston et al. 1995; Frick et al. 2004). Additionally, the non-calibrated V_m and Ca^{2+} signals still provide a unique possibility to analyse non-linear and spatially inhomogeneous interactions of dendritic membrane potential signals and Ca^{2+} signals that represent the first step in the induction of synaptic plasticity. This analysis is based on monitoring relative changes in V_m and Ca^{2+} signals from the same regions on the dendritic tree under different experimental conditions. In the experiment illustrated in Fig. 4e–g, V_m signals and Ca^{2+} transients were recorded sequentially from the same locations on the dendritic arbour. Specifically, we analysed a critical V_m signal that is spatially correlated with the supra-linear Ca^{2+} transient evoked by a theta-burst pairing protocol that typically induces LTP. Figure 4e shows that the EPSP related Ca^{2+} transient is strictly limited to the site of activated synapses (region 5). Figure 4f–g shows V_m and Ca^{2+} signals related to back-

propagating action potentials evoked alone (unpaired, black traces) and paired with a train of EPSPs (paired, red and blue traces) where the action potential was in coincidence with the fifth EPSP. Although a supra-linear Ca^{2+} signal was observed in different regions, only at location 5, adjacent to the stimulating electrode, it was mediated by NMDA receptors (see Fig. 6f in Canepari et al. 2007). The analysis of V_m and Ca^{2+} signals from this type of measurements resulted in the conclusion that unblocking of NMDA receptors during coincident activity and the resulting supra-linear increase in Ca^{2+} influx at the site of activated synapses did not require boosting of the back-propagating action potential baseline-to-peak amplitude as suggested in a number of previous studies (Canepari et al. 2007).

Combined Voltage and Ca^{2+} Imaging from Cerebellar Purkinje Neurons

As in pyramidal neurons, different patterns of synaptic activity can induce different forms of long-term synaptic plasticity in cerebellar Purkinje neurons. The associative signal for synaptic plasticity in the dendrites of Purkinje neurons that do not support back-propagating action potentials is the climbing fibre EPSP, a large synaptic potential originating in the soma and in the proximal dendrite. This signal spreads along the distal dendrites where the parallel fibre synapses are formed. Repetitive activation of parallel fibre synaptic activity can either induce LTP or long-term depression (LTD) depending on whether parallel fibre stimulation is paired with climbing fibre stimulation (Coesmans et al. 2004). Full understanding of synaptic mechanisms underlying parallel fibre synaptic plasticity requires spatially well-resolved recordings of both V_m and Ca^{2+} signals following different patterns of parallel fibre and climbing fibre activity.

To demonstrate the ability to carry out these experiments, we filled Purkinje neurons with 1 mM of the Ca^{2+} indicator Fura-FF and with the voltage sensitive dye JPW-1114. Purkinje neurons have an exceptionally high dendritic K_{cell} estimated at ~2,000 (Fierro and Llano 1996). Therefore, the addition of a low affinity Ca^{2+} indicator does not significantly alter the physiological homeostasis of Ca^{2+}, and Ca^{2+} signals can be quantified in terms of $\Delta[Ca^{2+}]_i$. Additionally, V_m $\Delta F/F$ signals can be calibrated in terms of membrane potential using long-lasting hyperpolarising pulses that have approximately the same amplitude throughout the dendritic arbor (Stuart and Häusser 1994; Roth and Häusser 2001). A standard calibration procedure is illustrated in Fig. 5. Figure 5a shows that the optical signal corresponding to 11.5 mV hyperpolarisation evoked in the soma is similar in different regions of the dendritic tree. The steady-state hyperpolarising pulse can be recorded at low acquisition rate (typically 125 frames/s) using a moderate illumination to minimise bleaching and photo-toxicity. These recordings are used to calibrate V_m signals at the level of single pixels.

Mature Purkinje neurons are characterised by a large EPSP driven by individual climbing fibres. The EPSP spreads from the sites of origin into more distal parts of the dendritic tree. To establish the sensitivity of V_m and Ca^{2+} imaging from Purkinje neurons, we monitored the climbing fibre EPSP at different distances from the soma. Recordings from four selected locations in Fig. 5b illustrate the signal-to-noise ratio which can be obtained with modest averaging (nine trials for V_m signals and four trials for Ca^{2+} signals). The calibrated optical signals indicated that the climbing fibre EPSP slightly attenuated along the dendrites but its amplitude remained at about 50 mV at 100 lm from the soma, in agreement with previous electrode recordings (Stuart and Häusser 1994). $\Delta[Ca^{2+}]_i$ signals associated with the climbing fibre EPSP and recorded sequentially from same locations slightly increased with distance from the soma. This result is not surprising given the uneven distribution of Ca^{2+} channels that increase with the distance from the soma (Llinas and Sugimori 1980).

In another series of measurements we used calibrated V_m and Ca^{2+} signals to analyse spatially non-uniform differences between dendritic signals associated with parallel fibre

and climbing fibre activation. Figure 5c shows a composite fluorescent image of a Purkinje neuron with three representative recording regions indicated by red boxes. The position of a stimulating electrode is shown schematically. A train of seven parallel fibre EPSPs at 100 Hz was evoked by stimulating a bundle of presynaptic fibres near the stimulating electrode. V_m signals (red traces) and $\Delta[Ca^{2+}]_i$ signals (blue traces) from three recording regions indicated in Fig. 4c are shown in Fig. 5d. The $\Delta[Ca^{2+}]_i$ signal with a peak amplitude of ~300 nM was strictly localised to the proximity of the stimulating electrode (location 1). The EPSP-evoked depolarisation preceding the Ca^{2+} signal at location 1 was ~60 mV in amplitude, markedly higher than the responses from the other two locations (<40 mV). This response was compared, in the same cell, with the depolarisation and $\Delta[Ca^{2+}]_i$ signal associated with a train of five climbing fibre EPSPs at 100 Hz. As shown in Fig. 5e, the climbing fibre stimulation protocol induced similar peak depolarisation (50–60 mV) in all three regions with a slight decline in the response during the train (black traces on the left). The membrane potential response was associated with a small $\Delta[Ca^{2+}]_i$ transient (<100 nM) corresponding to the first EPSP (Fig. 5f, black traces). At location 1 the peak depolarisation evoked by a train of climbing fibre EPSPs (black traces) was smaller compared to depolarisation evoked by parallel fibre activation (red traces) while at locations 2 and 3, the V_m response to climbing fibre stimulation was clearly larger in amplitude. We further established that $\Delta[Ca^{2+}]_i$ signals associated with activation of both parallel fibres and climbing fibres were mediated by voltage-gated Ca^{2+} channels. These signals were neither affected by the block of metabotropic glutamate receptors nor by the block of NMDA receptors, which are the only possible source of synaptic Ca^{2+} (data not shown). Thus, the remarkable regional difference between $\Delta[Ca^{2+}]_i$ signals evoked by parallel fibre and climbing fibre activation could be explained by differences in membrane potential responses and correlated with different short-term synaptic plasticity, (facilitation or depression) evoked by two synaptic pathways.

The comparison of both ΔV_m and $\Delta[Ca^{2+}]_i$ signals between different dendritic sites, as described above, depends on calibration of optical signals on an absolute scale. The combined V_m and Ca^{2+} imaging is the only approach currently available to carry out this type of measurements.

Discussion

Combining voltage and Ca^{2+} imaging is the only experimental approach that allows correlation of regional dendritic V_m and Ca^{2+} signals at multiple sites. This report describes the advantages and limitations of the technique as applied to the dendritic tree of individual mammal neurons in brain slices using UV-excitable Ca^{2+} indicators. In particular, it concentrates on the type of information that can be obtained from the application of this method depending on whether or not optical signals are calibrated.

If a voltage calibration is not available, the method is limited to monitoring relative changes in V_m signals under different conditions and to the analysis of the signal waveform which is obtained directly from the optical data. This type of measurements can provide unique and often critical information on synaptic potential and action potential signal interactions at high spatial and temporal resolution. If calibration of optical data in terms of membrane potential is possible, the amplitude of V_m signals from different dendritic regions can be compared on an absolute scale allowing quantitative analysis of how synaptic potentials and action potentials in the dendritic tree interact to control Ca^{2+} signalling, synaptic plasticity and input-output function of a neuron (Djurisic et al. 2004; Canepari et al. 2007).

Similar considerations apply to the interpretation of Ca^{2+} signals. If high concentrations of a high affinity Ca^{2+} indicator are used, the amplitude and the duration of $\Delta[Ca^{2+}]_i$ under

physiological conditions cannot be derived, but Ca^{2+} signals can be still used to characterise region specific non-linear Ca^{2+} responses that mediates synaptic plasticity (e.g. Koester and Sakmann 1998; Magee and Johnston 1997). If the endogenous Ca^{2+} buffering of the cell is high relative to the buffering capacity of the indicator, optical signals can be used to measure physiological $\Delta[Ca^{2+}]_i$ signals allowing the analysis of the relationship between spatial and temporal characteristics of $\Delta[Ca^{2+}]_i$ and synaptic plasticity.

Simultaneous Voltage and Ca^{2+} Imaging

UV-excitable Fura dyes are the optimal Ca^{2+} probes to be combined with styryl voltage-sensitive dyes because they have minimal overlap in the excitation and emission spectra. This combination, however, prevents the true simultaneous V_m and Ca^{2+} recordings which would be mandatory in measurements that depend on single trial recordings. The simultaneous V_m and Ca^{2+} imaging can be achieved by using two dedicated photo-detectors together with two fluorescent indicators with overlapping excitation spectra, but separable emission spectra. This approach, however, has reduced sensitivity compared to sequential recording because it requires several compromises including non-optimal excitation and emission wavelengths, an excess of photodynamic damage caused by continuous excitation of voltage-sensitive dye throughout the recording of longer-lasting Ca^{2+} signals, as well as the problem of incomplete optical separation of the emission spectra of the two indicators causing cross-talk between signals (Sinha et al. 1995; Bullen and Saggau 1998).

Present Limitations for In Vivo Imaging

A significant step forward in the experimental approach described here would be the possibility to combine dendritic V_m and Ca^{2+} optical recordings in vivo. At present, this possibility is limited, firstly by the difficulties of selective staining of individual neurons with voltage-sensitive dyes in vivo. Secondly, in vivo imaging from deep tissues with adequate spatial resolution requires non-linear optical methods (second-harmonic generation or two-photon fluorescence). The difficulties of recording fast (sub-millisecond) V_m transients with non-linear microscopy are considerable, precluding practical application of these techniques in physiologically relevant experiments. This was mainly because of the relatively small number of photons collected per time-point. In this situation, the high relative shot noise requires very high dye sensitivity (not currently available) to obtain detectable signals (Kuhn et al. 2004; Dombeck et al. 2005). Nevertheless, a recent improvement in the sensitivity of two-photon excitation V_m imaging, based on optimising several aspects of recording conditions, allowed, for the first time, recordings of action potentials in single-trial measurements from individual nerve terminals in mouse *in vivo* preparation (Fisher et al. 2008). This result provides methodological foundation for optical monitoring of electrical activity *in vivo* that could be combined with two-photon Ca^{2+} imaging.

Acknowledgments

This work was supported by the University of Basel and the NIH Grant RO1NS42739. We are grateful to Leslie Loew and Joe Wuskel for kindly providing voltage-sensitive dyes, and to Helene Pierre for technical help.

References

Antic S. Action potentials in basal and oblique dendrites of rat neocortical pyramidal neurons. J Physiol (Lond). 2003; 550:35–50. [PubMed: 12730348]

Antic S, Zecevic D. Optical signals from neurons with internally applied voltage-sensitive dyes. J Neurosci. 1995; 15:1392–1405. [PubMed: 7869106]

Antic S, Major G, Zecevic D. Fast optical recordings of membrane potential changes from dendrites of pyramidal neurons. J Neurophysiol. 1999; 82:1615–1621. [PubMed: 10482775]

Antic S, Wuskell JP, Loew L, Zecevic D. Functional profile of the giant metacerebral neuron of Helix aspersa: temporal and spatial dynamics of electrical activity in situ. J Physiol (Lond). 2000; 527:55–69. [PubMed: 10944170]

Berger T, Borgdorff A, Crochet S, Neubauer FB, Lefort S, Fauvet B, Ferezou I, Carleton A, Luscher HR, Petersen CC. Combined voltage and calcium epifluorescence imaging in vitro and in vivo reveals subthreshold and suprathreshold dynamics of mouse barrel cortex. J Neurophysiol. 2007; 97:3751–3762. [PubMed: 17360827]

Bischofberger J, Jonas P. Action potential propagation into the presynaptic dendrites of rat mitral cells. J Physiol (Lond). 1997; 504:359–365. [PubMed: 9365910]

Borst JG, Helmchen F, Sakmann B. Pre- and postsynaptic whole-cell recordings in the medial nucleus of the trapezoid body of the rat. J Physiol (Lond). 1995; 489:825–840. [PubMed: 8788946]

Bullen A, Saggau P. Indicators and optical configuration for simultaneous high-resolution recording of membrane potential and intracellular calcium using laser scanning microscopy. Pflügers Arch. 1998; 436:788–796.

Canepari M, Mammano F. Imaging neuronal calcium fluorescence at high spatio-temporal resolution. J Neurosci Meth. 1999; 87:1–11.

Canepari M, Auger C, Ogden D. Ca^{2+} ion permeability and single-channel properties of the metabotropic slow EPSC of rat Purkinje neurons. J Neurosci. 2004; 24:3563–3573. [PubMed: 15071104]

Canepari M, Djurisic M, Zecevic D. Dendritic signals from rat hippocampal CA1 pyramidal neurons during coincident pre- and post-synaptic activity: a combined voltage- and calcium imaging study. J Physiol (Lond). 2007; 580:463–484. [PubMed: 17272348]

Cohen LB, Salzberg BM, Davila HV, Ross WN, Landowne D, Waggoner AS, Wang CH. Changes in axon fluorescence during activity: molecular probes of membrane potential. J Membr Biol. 1974; 19:1–36. [PubMed: 4431037]

Coesmans M, Weber JT, De Zeeuw CI, Hansel C. Bidirectional parallel fiber plasticity in the cerebellum under climbing fiber control. Neuron. 2004; 44:691–700. [PubMed: 15541316]

Djurisic M, Antic S, Chen WR, Zecevic D. Voltage imaging from dendrites of mitral cells: EPSP attenuation and spike trigger zones. J Neurosci. 2004; 24:6703–6714. [PubMed: 15282273]

Dombeck DA, Sacconi L, Blanchard-Desce M, Webb WW. Optical recording of fast neuronal membrane potential transients in acute mammalian brain slices by second-harmonic generation microscopy. J Neurophysiol. 2005; 94:3628–3636. [PubMed: 16093337]

Fierro L, Llano I. High endogenous calcium buffering in Purkinje cells from rat cerebellar slices. J Physiol (Lond). 1996; 496:617–625. [PubMed: 8930830]

Fisher JA, Barchi JR, Welle CG, Kim GH, Kosterin P, Obaid AL, Yodh AG, Contreras D, Salzberg BM. Two-photon excitation of potentiometric probes enables optical recording of action potentials from mammalian nerve terminals in situ. J Neurophysiol. 2008; 99:1545–1553. [PubMed: 18171710]

Frick A, Magee J, Johnston D. LTP is accompanied by an enhanced local excitability of pyramidal neuron dendrites. Nat Neurosci. 2004; 7:126–135. [PubMed: 14730307]

Gasparini S, Losonczy A, Chen X, Johnston D, Magee JC. Associative pairing enhances action potential back-propagation in radial oblique branches of CA1 pyramidal neurons. J Physiol (Lond). 2007; 580:787–800. [PubMed: 17272353]

Grinvald A, Salzberg BM, Lev-Ram V, Hildesheim R. Optical recording of synaptic potentials from processes of single neurons using intracellular potentiometric dyes. Biophys J. 1987; 51:643–651. [PubMed: 3580490]

Helmchen F, Imoto K, Sakmann B. Ca^{2+} buffering and action potential-evoked Ca^{2+} signaling in dendrites of pyramidal neurons. Biophys J. 1996; 70:1069–1081. [PubMed: 8789126]

Hyrc KL, Bownik JM, Goldberg MP. Ionic selectivity of low-affinity ratiometric calcium indicators: mag-Fura–2, Fura-2FF and BTC. Cell Calcium. 2000; 27:75–86. [PubMed: 10756974]

Jackson MB, Redman SJ. Calcium dynamics, buffering, and buffer saturation in the boutons of dentate granule-cell axons in the hilus. J Neurosci. 2003; 23:1612–1621. [PubMed: 12629165]

Kaiser KM, Zilberter Y, Sakmann B. Back-propagating action potentials mediate calcium signalling in dendrites of bitufted interneurons in layer 2/3 of rat somatosensory cortex. J Physiol (Lond). 2001; 535:17–31. [PubMed: 11507155]

Koester HJ, Sakmann B. Calcium dynamics in single spines during coincident pre- and postsynaptic activity depend on relative timing of back-propagating action potentials and subthreshold excitatory postsynaptic potentials. Proc Natl Acad Sci USA. 1998; 95:9596–9601. [PubMed: 9689126]

Kremer SG, Zeng W, Skorecki KL. Simultaneous fluorescence measurement of calcium and membrane potential responses to endothelin. Am J Physiol. 1992; 263:1302–1309.

Kuhn B, Fromherz P, Denk W. High sensitivity of Stark-shift voltage-sensing dyes by one- or two-photon excitation near the red spectral edge. Biophys J. 2004; 87:631–639. [PubMed: 15240496]

Jaffe DB, Johnston D, Lasser-Ross N, Lisman JE, Miyakawa H, Ross WN. The spread of Na^+ spikes determines the pattern of dendritic Ca^{2+} entry into hippocampal neurons. Nature. 1992; 357:244–246. [PubMed: 1350327]

Lips MB, Keller BU. Endogenous calcium buffering in motoneurones of the nucleus hypoglossus from mouse. J Physiol (Lond). 1998; 511:105–117. [PubMed: 9679167]

Llinas R, Sugimori M. Electrophysiological properties of in vitro Purkinje cell dendrites in mammalian cerebellar slices. J Physiol (Lond). 1980; 305:197–213. [PubMed: 7441553]

Loew LM, Simpson LL. Charge-shift probes of membrane potential: a probable electrochromic mechanism for p-aminostyrylpyridinium probes on a hemispherical lipid bilayer. Biophys J. 1981; 34:353–365. [PubMed: 7248466]

Loew LM, Cohen LB, Dix J, Fluhler EN, Montana V, Salama G, Wu JY. A naphthyl analog of the aminostyryl pyridinium class of potentiometric membrane dyes shows consistent sensitivity in a variety of tissue, cell, and model membrane preparations. J Membr Biol. 1992; 130:1–10. [PubMed: 1469705]

Magee JC, Johnston D. A synaptically controlled, associative signal for Hebbian plasticity in hippocampal neurons. Science. 1997; 275:209–213. [PubMed: 8985013]

Martinez-Zaguilan R, Martinez GM, Lattanzio F, Gillies RJ. Simultaneous measurement of intracellular pH and Ca^{2+} using the fluorescence of SNARF-1 and fura-2. Am J Physiol. 1991; 260:297–307.

Milojkovic BA, Radojicic MS, Antic SD. A strict correlation between dendritic and somatic plateau depolarizations in the rat prefrontal cortex pyramidal neurons. J Neurosci. 2005; 25:3940–3951. [PubMed: 15829646]

Milojkovic BA, Zhou WL, Antic SD. Voltage and calcium transients in basal dendrites of the rat prefrontal cortex. J Physiol (Lond). 2007; 585:447–468. [PubMed: 17932150]

Naraghi M. T-jump study of calcium binding kinetics of calcium chelators. Cell Calcium. 1997; 22:255–268. [PubMed: 9481476]

Neher E. The use of fura-2 for estimating Ca buffers and Ca fluxes. Neuropharmacology. 1995; 34:1423–1442. [PubMed: 8606791]

Nowycky MC, Pinter MJ. Time courses of calcium and calcium-bound buffers following calcium influx in a model cell. Biophys J. 1993; 64:77–91. [PubMed: 8431551]

Ogden D, Capiod T. regulation of Ca^{2+} release by InsP3 in single guinea pig hepatocytes and rat Purkinje neurons. J Gen Physiol. 1997; 109:741–756. [PubMed: 9222900]

Palecek J, Lips MB, Keller BU. Calcium dynamics and buffering in motoneurones of the mouse spinal cord. J Physiol (Lond). 1999; 520:485–502. [PubMed: 10523417]

Palmer LM, Stuart GJ. Site of action potential initiation in layer 5 pyramidal neurons. J Neurosci. 2006; 26:1854–1863. [PubMed: 16467534]

Roth A, Häusser M. Compartmentalmodels of rat cerebellar Purkinje cells based on simultaneous somatic and dendritic patch-clamp recordings. J Physiol (Lond). 2001; 535:445–472. [PubMed: 11533136]

Sabatini BS, Oertner TG, Svoboda K. The life cycle of Ca^{2+} ions in dendritic spines. Neuron. 2002; 33:439–452. [PubMed: 11832230]

Sacconi L, Dombeck DA, Webb WW. Overcoming photodamage in second-harmonic generation microscopy: real-time optical recording of neuronal action potentials. Proc Natl Acad Sci USA. 2006; 103:3124–3129. [PubMed: 16488972]

Schneggenburger R, Meyer AC, Neher E. Released fraction and total size of a pool of immediately available transmitter quanta at a calyx synapse. Neuron. 1999; 23:399–409. [PubMed: 10399944]

Sinha SR, Saggau P. Simultaneous optical recording of membrane potential and intracellular calcium from brain slices. Methods. 1999; 18:204–214. [PubMed: 10356352]

Sinha SR, Patel SS, Saggau P. Simultaneous optical recording of evoked and spontaneous transients of membrane potential and intracellular calcium concentration with high spatio-temporal resolution. J Neurosci Meth. 1995; 60:49–60.

Spruston N, Schiller Y, Stuart G, Sakmann B. Activity-dependent action potential invasion and calcium influx into hippocampal CA1 dendrites. Science. 1995; 268:297–300. [PubMed: 7716524]

Stuart G, Häusser M. Initiation and spread of sodium action potentials in cerebellar Purkije neurons. Neuron. 1994; 13:703–712. [PubMed: 7917300]

Vanselow BK, Keller BU. Calcium dynamics and buffering in oculomotor neurones from mouse that are particularly resistant during amyotrophic lateral sclerosis (ALS)-related motoneurone disease. J Physiol (Lond). 2000; 525:433–445. [PubMed: 10835045]

Wang J, Yeckel MF, Johnston D, Zucker RS. Photolysis of postsynaptic caged Ca2+ can potentiate and depress mossy fiber synaptic responses in rat hippocampal CA3 pyramidal neurons. J Neurophysiol. 2001; 91:1596–1607. [PubMed: 14645386]

Zecevic D. Multiple spike-initiation zones in single neurons revealed by voltage-sensitive dyes. Nature. 1996; 381:322–325. [PubMed: 8692270]

Zhou W-L, Yan P, Wuskell JP, Loew LM, Antic SD. Intracellular long-wavelength voltage-sensitive dyes for studying the dynamics of action potentials in axons and thin dendrites. J Neurosci Meth. 2007; 164:225–239.

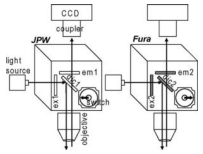

Fig. 1.

Schematic of the imaging apparatus. Imaging set-up for sequential recording of V_m and Ca^{2+} signals in epi-fluorescence mode by switching between two filter cubes. Filter set for voltage-sensitive dye (JPW): ex1 = 525 ± 25 nm, dic1 > 570 nm and em1 > 610 nm. Filter set for Ca^{2+} indicator (Fura): ex2 = 387 ± 6 nm, dic1 > 470 nm and em1 = 510 ± 42 nm

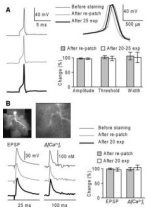

Fig. 2.

Pharmacological effects and photodynamic damage of JPW-1114 in cerebellar Purkinje neurons. (**a**) Electrode recordings of the AP from the soma at the beginning of the staining (thin-black trace), after re-patch (grey trace) and after 25 optical recordings of 150 ms separated by 30 s (thick-black trace). Graph: summary data for spike amplitude, voltage threshold, and width at half-height after staining (grey bars) and optical recordings (white bars) expressed as percent changes from control values (*N* = 4 cells). (**b**) Top left: a composite fluorescence image of a Purkinje neuron. Top right: fluorescence image of a dendritic region in the recording position. *Bottom left*: electrically recorded somatic climbing fibre EPSP and associated $\Delta[Ca^{2+}]_i$ signal from the dendrite shown above at the beginning of the staining (thin-black trace), after re-patch (grey trace) and after 20 optical recordings of 150 ms separated by 30 s (thick-black trace); $\Delta[Ca^{2+}]_i$ signal estimated by averaging fluorescence over the entire dendritic area of the top-right image. *Bottom right*: summary data for the EPSP and $\Delta[Ca^{2+}]_i$ amplitude after staining (grey bars) and optical recordings (white bars) expressed as per cent changes from control values (*N* = 5 cells)

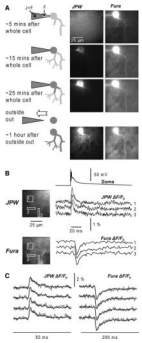

Fig. 3.

Staining of the cells and recording procedures. (**a**) A Purkinje neuron loading with a voltage sensitive dye (JPW, left column) and a Ca^{2+} indicator (Fura, right column). The internal solution in the tip of the patch electrode did not contain voltage sensitive dye. Images were taken at 5, 15 and 25 min after whole-cell configuration and 1 h after the patch electrode was removed. (**b**) V_m and Ca^{2+} fractional changes of fluorescence related to a climbing fibre EPSP recorded after the dye equilibration period from the locations 1–3 reported in the fluorescence images of the dendritic tree on the left. Somatic recording of the climbing fibre EPSP is the upper trace. Four trials averaged to improve the signal-to-noise ratio. (**c**) Individual recordings of V_m (left) and Ca^{2+} (right) fractional changes of fluorescence (grey traces) related to a climbing fibre EPSP. Superimposed black traces are the averages of the four trials

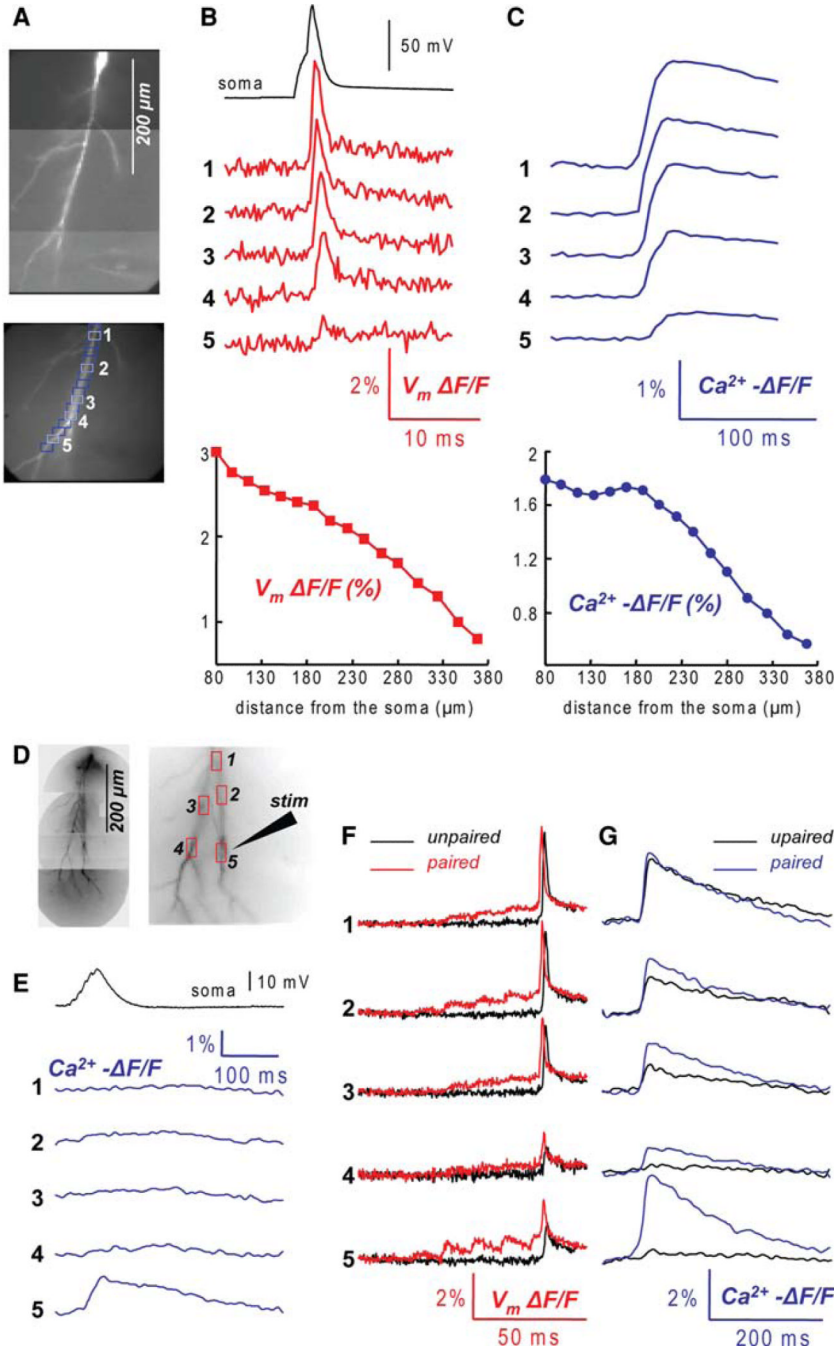

Fig. 4.

Combined voltage and Ca^{2+} imaging from CA1 hippocampal pyramidal neurons. (**a**) A composite fluorescence image of a hippocampal CA1 pyramidal neuron (top) and a fluorescence image of an apical dendrite of the same cell in recording position (bottom); 16 regions at different distance from the soma marked by blue rectangles. (**b**) V_m signals ($\Delta F/F$) from locations 1–5 associated with a back-propagating action potential. Somatic recording of the action potential is the upper black trace, a plot of signal amplitude vs. distance from the soma shown below. (**c**) Ca^{2+} signal ($-\Delta F/F$) from locations 1–5 associated with a back-propagating action potential. A plot of signal amplitude vs distance from the soma shown below. (**d**) A composite fluorescence image of another CA1 pyramidal neuron

(left) and fluorescence image of the dendritic tree of the same cell in recording position (right). An extracellular stimulating electrode shown schematically. Five recording locations marked by red rectangles. (**e**) Ca^{2+} signals from locations 1–5 associated with a train of 5 EPSPs at 100 Hz. Note that the Ca^{2+} transient was localised to region 5. Somatic recording of the EPSPs is the upper black trace. (**f**) V_m signals from locations 1–5 associated with a back-propagating action potential (black traces) and with the pairing of 5 EPSPs with a back-propagating action potential (red traces). (**g**) Ca^{2+} signals from locations 1–5 associated with a back-propagating action potential (black traces) and with the pairing protocol (blue traces). V_m signals obtained at frame rate of 5 kHz. Ca^{2+} signals obtained at frame rate of 500 Hz

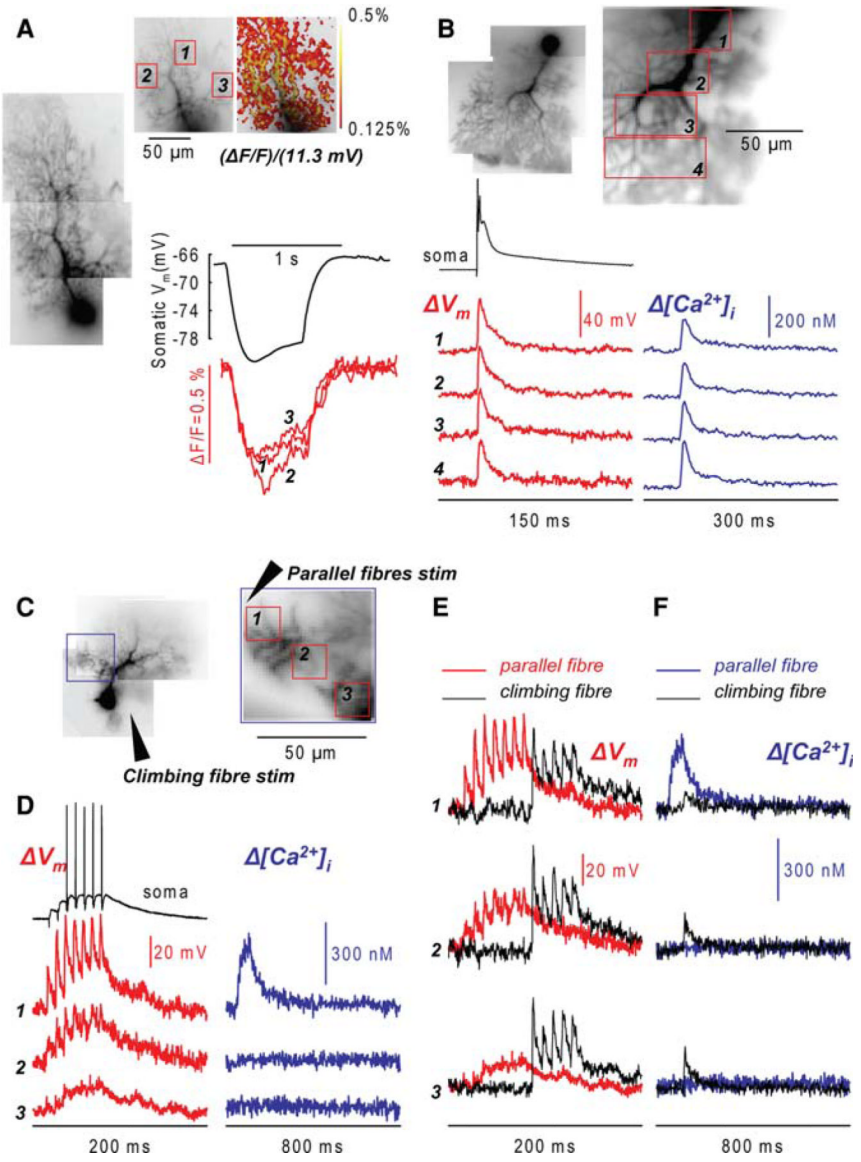

Fig. 5.

Combined voltage and Ca^{2+} imaging from cerebellar Purkinje neurons. (**a**) Calibration of V_m signals. A composite fluorescence image of a Purkinje neuron (left) and a fluorescence images of the dendritic tree in recording position with three recording locations marked by red rectangles (top). The colour-coded representation of the optical signal corresponding to 11.5 mV prolonged somatic hyperpolarisation (top right). Electrical recording from the soma (black trace) and optical recordings from three marked locations (red traces) shown below. (**b**) A composite fluorescence image of another Purkinje neuron (top left) and a region on the dendritic tree in recording position with four recording locationsmarked byred rectangles(top right). V_m signals (ΔV_m, red traces—average of nine recordings) and Ca^{2+} signals ($\Delta[Ca^{2+}]_i$ blue traces—average of four recordings) from locations 1 to 4 associated with a climbing fibre EPSP (bottom). Somatic recording is the upper black trace. (**c**) A composite fluorescence image of a Purkinje neuron (left) and an image of a dendritic region in recordingposition with three locations marked byred rectangles; the position of the dendritic region in the composite image marked by a blue rectangle. Two stimulating electrodes for the parallel fibres and the climbing fibre depicted schematically. (**d**) V_m

signals (red traces—average of four recordings) and Ca^{2+} signals (blue traces—average of four recordings) associated with a train ofseven parallel fibre EPSPs at 100 Hz. Localised Ca^{2+} signal at location 1 corresponds spatially to the largest depolarisation. Somatic recording is the upper black trace. (**e**) V_m signals from locations 1–3 associated with a train of five climbing fibre EPSPs (black traces) and with a train of seven parallel fibre EPSPs (red traces).(**f**) Ca^{2+} signals from locations 1–3 associated with a train of five climbing fibre EPSPs (black traces) and with a train of seven parallel fibre EPSPs (blue traces). V_m signals obtained at frame rate of 2 kHz. Ca^{2+} signals obtained at frame rate of 500 Hz

Table 1

Dissociation constants and buffering capacities of Fura dyes. A list of commercially available Fura dyes with dissociation constant (K_d) and buffering capacities (K_{dye}) at the two concentrations of 300 μM and 1 mM

Dye	K_d (μM)	K_{dye} (300 μM)	K_{dye} (1 mM)
Fura-2	0.224[a]	~1300	~4500
Fura-5F	0.4[a]	~750	~2500
Bis-fura-2	0.525[a]	~570	~1900
Fura-4F	0.77[a]	~390	~1300
Fura-6F	5.3[a]	~57	~190
Fura-FF	10[b]	~30	~100
Mag-fura-2	25[c]–10[d]	~7.5–12	~25–40

References:

[a] Molecular Probes handbook (for fura-2 and bis-fura-2 at 1 mM Mg^{2+})

[b] Schneggenburger et al. (1999)

[c] Hyrc et al. (2000)

[d] Naraghi (1997)

Table 2

Endogenous buffering capacities of some neurons. Estimated endogenous buffering capacities (K_{cell}) of some rodent neurons

CNS region	Neuron type	Site	K_{cell}
Hippocampus CA1	Pyramidal	Spine	~20[a]
Hippocampus DG	Granule	Axon	~20[b]
MNTB	Calyx Held	Axon	~40[c]
Hypoglossum	Motoneuron	Soma	~41[d]
Spinal Cord	Motoneuron	Soma	~50[e]
Neocortex L5	Pyramidal	Dendr.	~130[f]
Hippocampus CA1	Pyramidal	Dendr.	~180[f]
OM nucleus	Motoneuron	Soma	~265[g]
Neocortex L2/3	Bitufted i.n.	Dendr.	~285[h]
Hippocampus CA3	Pyramidal	Dendr.	~900[i]
Cerebellum	Purkinje	Dendr.	~2000[j]

References:

[a] Sabatini et al. (2002)

[b] Jackson and Redman (2003)

[c] Borst et al. (1995)

[d] Lips and Keller (1998)

[e] Palecek et al. (1999)

[f] Helmchen et al. (1996)

[g] Vanselow and Keller (2000)

[h] Kaiser et al. (2001)

[i] Wang et al. (2001)

[j] Fierro and Llano (1996)